Polarized Infrared Absorption Spectra of Matrix-Isolated Allyl Radicals

Sreela Nandi,[†] Pamela A. Arnold,[‡] Barry K. Carpenter,*[,‡] Mark R. Nimlos,*[,†,§] David C. Dayton,[§] and G. Barney Ellison*[,†,||]

Department of Chemistry and Biochemistry, University of Colorado, Boulder, Colorado 80309-0215, Department of Chemistry, Cornell University, Ithaca, New York 14853, and National Renewable Energy Laboratory, 1617 Cole Boulevard, Golden, Colorado 80401

Received: March 28, 2001; In Final Form: May 21, 2001

We have measured the polarized infrared absorption spectrum of the allyl radical, CH_2CHCH_2 ($\tilde{X}$) $^2A_2$, in an argon matrix at 10 K. The experimental CH_2CHCH_2 frequencies (cm^{-1}) and polarizations follow: a_1 modes, 3109, 3052, 3027, 1478, and 1242; b_1 modes, 983, 801, and 510; b_2 modes, 3107, 3020, 1464, 1390, and 1182. Two modes (ν_6 and ν_{18}) are very weak and could not be detected; the lowest frequency a_1 mode (the $CH_2-CH-CH_2$ bending mode ν_7) is estimated to be beyond the wavelength range of our MCT infrared detector. Infrared absorption spectra of two deuterated isotopomers, CH_2CDCH_2 and CD_2CDCD_2, were recorded in order to compare experimental frequency shifts with calculated [UB3LYP/6-311-G(d,p)] harmonic frequencies. Linear dichroism spectra were measured with photooriented samples in order to establish experimental polarizations of most vibrational bands. True gas-phase vibrational frequencies were estimated by considering the gas-to-matrix shifts and matrix inhomogeneous line broadening. The allyl radical matrix frequencies listed above are within ±1% of the gas-phase vibrational frequencies. A final experimental set of all the vibrational frequencies for the allyl radical are recommended. See also: http://ellison.colorado.edu/allyl.

I. Introduction

The allyl radical, CH_2CHCH_2, is one of the simplest conjugated hydrocarbon radicals. It is commonly depicted as [$CH_2-CH=CH_2 \leftrightarrow CH_2=CH-CH_2$] and is used as an example of resonance.[1,2] The stabilization of the allyl radical is generally reckoned[3,4] to be roughly 40 kJ mol^{-1} (10 kcal mol^{-1}). As a consequence of the importance of this resonance stabilization, the thermochemistry of CH_2CHCH_2 (plus the ions, $CH_2CHCH_2^+$ and $CH_2CHCH_2^-$) has been carefully studied. The adiabatic ionization potential was originally has been measured[5] via classical photoelectron spectroscopy as $IP(CH_2CHCH_2) = 8.13 \pm 0.02$ eV. The allyl's ionization potential has recently been redetermined via a Rydberg extrapolation[6] to be $IP(CH_2CHCH_2) = 65\,638 \pm 18$ cm^{-1} [or 8.138 ± 0.002 eV] which differs slighly from a ZEKE measurement[7,8] of $IP(CH_2CHCH_2) = 65\,762 \pm 5$ cm^{-1} [8.1535 ± 0.0006 eV]. The adiabatic electron affinity[9,10] is $EA(CH_2CHCH_2) = 0.581 \pm 0.008$ eV. The bond energy for propene has been carefully measured to be $D_0(CH_2-CHCH_2-H) = 365.7 \pm 1.7$ kJ mol^{-1} (87.4 ± 0.4 kcal mol^{-1}), and the bond enthalpy[3] is $DH_{298}(CH_2CHCH_2-H) = 371.5 \pm 1.7$ kJ mol^{-1} (88.4 ± 0.4 kcal mol^{-1}). These bond dissociation energies imply $\Delta_f H_0(CH_2CHCH_2) = 184.5 \pm 2.1$ kJ mol^{-1} and $\Delta_f H_{300}(CH_2CHCH_2) = 173.2 \pm 1.7$ kJ mol^{-1}. Since the bond energy of cyclopropane,[11] c-C_3H_5, has been reported to be $DH_{298}(c\text{-}C_3H_5-H) = 444 \pm 13$ kJ mol^{-1} (106 ± 3 kcal mol^{-1}), one can estimate that the rearrangement of the cyclopropyl radical to allyl radical will be exothermic by roughly 1.4 eV.

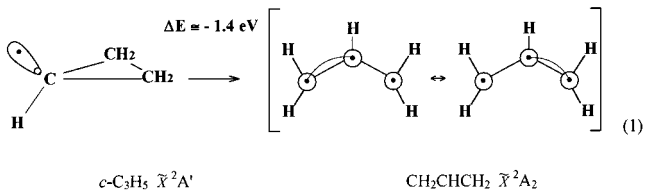

(1)

In this paper we report the infrared absorption spectrum of CH_2CHCH_2 ($\tilde{X}$) $^2A_2$. There have been many previous studies of the vibrational spectrum of allyl but they are incomplete and somewhat contradictory. Over the past few years we have developed a convenient hyperthermal nozzle to prepare matrix isolated organic radicals.[12,13] We have used this intense radical source to prepare matrix isolated samples of the three isotopic variants of the allyl: CH_2CHCH_2, CH_2CDCH_2, and CD_2CDCD_2. Following preparation of the target allylic radicals, we have used a Fourier transform infrared spectrometer (FTIR) to measure the infrared absorption spectra of these species. With the help of a polarized laser, the linear dichroism spectrum was measured with photooriented samples in order to establish experimental polarizations of most of the vibrational bands of the allyl radical

II. Experimental Section

A. Radical Beam and Infrared Spectroscopy. Most matrix-isolated radicals are prepared by photodissociation of an appropriate precursor (usually by a laser). A drawback of this procedure is that the target radical is almost always photochemically active and suffers photofragmentation. Consequently, as fast at the laser generates the target radical, it may also destroy it. Thus, we have resorted to high-temperature flash pyrolysis (850 °C) of thermally labile precursors. We produce the allyl

* To whom correspondence should be addressed.
† Department of Chemistry and Biochemistry.
‡ Department of Chemistry.
§ National Renewable Energy Laboratory.
|| E-mail: barney@jila.colorado.edu.

10.1021/jp011163s CCC: $20.00
Published on Web 07/12/2001

radical in the gas phase by pyrolysis of a suitable precursor molecule in a hyperthermal, supersonic jet expansion. The hyperthermal dosing nozzle is interfaced with a commercial APD two stage closed-cycle helium cryostat that is maintained at 25 K. CH_2CHCH_2 radicals are deposited onto a cold CsI window and detected using a Nicolet Magna 550 FTIR. The IR detectors are mercury−cadmium-telluride sensors; the MCT-A which has a detection range from 4000 to 600 cm^{-1} and while the MCT-B has a detection range from 4000 to 400 cm^{-1} and a much lower sensitivity. Polarized laser light for photoorientation experiments is generated at 351 nm from a Coherent Innova 200/25 CW Argon ion laser. Polarized IR light is generated using a Molectron wire grid IR polarizer.

The hyperthermal supersonic nozzle used in our experiments is a modified version of the nozzle developed in the laboratory of Peter Chen.[14] Our version[12,13] consists of a Series 9 Parker General Valve pulsed solenoid valve (0.1 mm diam) followed by a concentric 1 mm silicon carbide tube. The resistively heated silicon carbide tube is connected through two carbon electrodes to the output of a Love Control microprocessor-based temperature controller (model 16A3051). The temperature is monitored using a type C thermocouple attached to the center of the silicon carbide tube, which continuously supplies feedback to the controller unit; typical operating temperatures[13] are roughly 1150 K. This control system maintains the temperature steady within typically ±1 K over the course of an experiment. The length of the heated region of the silicon carbide tube is approximately 2 cm. The residence times in the heated region of the hyperthermal nozzle are estimated to be less than 100 μs. Residence times are believed to increase as pyrolysis temperature increases.[15] The output of the nozzle is directed toward a cryogenic matrix window and the radicals entrained in the molecular beam are frozen onto the cryogenic substrate. Dosing times are typically 3−4 h.

This work focuses on the infrared spectrum of the allyl radical parent and two of its deuterated isotopomers, CH_2CDCH_2 and CD_2CDCD_2. Precursors used to produce the allyl radical included $CH_2{=}CHCH_2I$, $CH_2{=}CHCH_2Br$, $CH_2{=}CHCH_2S_2CH_2$-$CH{=}CH_2$, and $CH_2{=}CHCH_2CH_2CH{=}CH_2$ which were supplied by Aldrich Chemical Co. The appropriate deuterated allyl iodides, $CH_2{=}CDCH_2I$ and $CD_2{=}CDCD_2I$, were synthesized as described below. All precursors afforded us samples of the allyl radical but some were better than others. We observed near complete depletion (roughly 90−95%) of the 1,5-hexadiene and allyl iodide precursors in the hyperthermal nozzle. Vibrational frequencies and intensities were matched for the different precursors used. Spectra shown in this work are from the allyl iodide precursor.

Gas mixtures were primarily argon seeded with a suitable radical precursor. These gas mixtures were made by sampling the vapor of the de-gassed precursor liquid at ambient temperature. Higher vapor pressure contaminants such as CH_3OCH_3 or CH_3I became enriched in the dosing mixture. $CH_2{=}CHCH_2S_2$-$CH_2CH{=}CH_2$ and $CH_2{=}CHCH_2CH_2CH{=}CH_2$ will decompose to produce two allyl radical and were used in approximately half the concentration compared to the other precursors. Gas mixtures were made in a 300 mL or a 1.3 L reservoir; deposition quantities and dosing rates were determined by monitoring pressure drop in the reservoir. We pulsed the dosing nozzle at a repetition rate of 30 to 10 Hz in order not to exceed the pumping speed of our system. Valve-opening times were 150−300 μs. A hyperthermal nozzle firing at 30 Hz for 150 μs produces about 10^{18} Ar atoms s^{-1} and roughly 10^{15} CH_2CHCH_2 radicals s^{-1} at the 25 K CsI window of the cryostat as estimated from choked flow at the 0.1 mm orifice.

B. PIMS Spectroscopy as a Radical Diagnostic. One of the experimental difficulties of matrix-isolated radical spectroscopy is to devise and optimize a clean source of radicals. The hyperthermal nozzle has been shown by Chen[14] to be an excellent radical source which he developed using a photoionization mass spectrometer (PIMS) to monitor and adjust the radical beam. We have adopted a PIMS as well in order to optimize our allyl radical source.

Prior to matrix deposition for an FTIR study, the optimal parameters for clean CH_2CHCH_2 radical production in the dosing nozzles was determined by monitoring products in a reflectron time-of-flight photoionization mass spectrometer. The mass spectrometer used in this experiment is a commercial RM Jordan reflectron TOF instrument that has been described in detail previously.[16] The output of the hyperthermal dosing jet is allowed to expand for approximately 1 cm and is skimmed before the molecular beam enters a laser interaction chamber. In the laser interaction region, an orthogonally orientated beam of 118.2 nm light (10.487 eV) crosses the molecular beam, ionizing the molecules entrained in the beam with ionization potential less than 10.5 eV. Positive ions are deflected by a positively biased deflector plate and injected through a pinhole into a time-of-flight mass analyzer. Ions are mass selected by a reflectron analyzer[17] and detected at off-axis microchannel plates.

Tripling[18] the third harmonic of a Nd:YAG laser in a xenon tripling cell generates the ($3 \times 3 \times 1.064$ μm^3) 118.2 nm laser pulse. The 118.2 nm light is focused at the interaction region while the nontripled 532 nm light diverges. The laser has a fixed repetition rate of 10 Hz and provides the timing trigger for the experiment.

Before introduction of the thermally dissociated gas mixture, the instrument was calibrated with propylene (m/z 42) or other simple hydrocarbons mixed with an inert gas. The parameters of the hyperthermal nozzle were then adjusted to the point where only the desired radical ion and leaving group ion are detected. Note that the peak intensities are not a reflection of the relative amounts of species present. Peak heights depend on both detection efficiencies and photoionization cross sections. Detection efficiencies are a function of particle mass and momentum. Photoionization cross sections are dependent[19] on the species' ionization potential and vibrational excitation.

C. Chemical Synthesis of Allyl Radical Precursors. To produce samples of CH_2CDCH_2 and CD_2CDCD_2, the corresponding allylic iodides were required; these compounds were synthesized. A dry 250 mL round-bottomed, three-necked flask was equipped with a condenser, an addition funnel, and a stir bar. The flask was charged with 1.20 g (28.6 mmol) of lithium aluminum deuteride, 3.09 g (57.2 mmol) of sodium methoxide, and 90 mL of freshly distilled diethyl ether. The mixture was cooled in an ice bath while propargyl alcohol, $HC{\equiv}CCH_2OH$ (1.5 mL, 25.8 mmol), in 60 mL of ether was added dropwise from the addition funnel over 1 h. The reaction mixture was heated to reflux for 52 h, then cooled in an ice bath and quenched by addition of 5 mL of water. After stirring for 4 h, the reaction mixture was filtered through a glass frit. Ether was distilled from the filtrate at atmospheric pressure with a short-path distillation head. The remaining material was then fractionally distilled. Allyl-2-d_1 alcohol, $CH_2{=}CDCH_2OH$, was collected as a colorless oil at 96−105 °C (45% yield). ^1H NMR (400 MHz, C_6D_6) δ 3.80 (s), 4.95 (m), 5.14 (m).

TABLE 1: Previously Measured CH_2CHCH_2 Vibrational Fundamentals

		review[55]	matrix FTIR[41]	matrix FTIR[43]	matrix FTIR[39]	matrix FTIR[40]	MPI[34]	Rydberg[6]	resonance Raman[35]	laser absorption[27]	laser absorption[25]	laser absorption[26]	negative ion PES[10]
a_1	ν_1		3105	3107	3109			3212			3113.98488 ±0.00089	3113.9779 ±0.0003	
	ν_2	3048	3048	3051, 3040	3051			3109					
	ν_3		3016	3019	3019			3104					
	ν_4	1488, 1477	1463	1463	1478			1504	1487				
	ν_5	1245, 242	1403	1242, 1182	1242			1268	1246				
	ν_6	1066	1242	972.8	1183			1032	1068				990
	ν_7	427	511	510			426	423	429				425
a_2	ν_8							705					
	ν_9	549					558	552	549				
b_1	ν_{10}	968, 983.6	985	808.5	984	983.6		1001	968 ($2\nu_{10}$)				
	ν_{11}	801.7	810	801.2	802	801.1		721		801.71909 ±0.00037			800
	ν_{12}	518, 510.1	802		511	510.1	508 ± 12	516	518 ($2\nu_{12}$)				
b_2	ν_{13}	3105	3105	3107	3109			3210			3110.59857 ±0.00036	3110.5	
	ν_{14}	3016	3016	3019	3019			3100					
	ν_{15}	1463	1477	1477	1464			1467					
	ν_{16}	1389	1463	1389, 1317	1389			1382					
	ν_{17}	1182	1389	1284	1284			1104					
	ν_{18}		1285	983.2	810			918					
						Previously Measured CD_2CDCD_2 Fundamentals							
a_1	ν_1												
	ν_2	2285		2285									
	ν_3	2215		2214									
	ν_4	1272, 1263		1018									
	ν_5	1020, 1018, 1007								1020			
	ν_6	844							1272				835
	ν_7								350, 357				345
a_2	ν_8												
	ν_9								372 ($2\nu_9$)				
b_1	ν_{10}	767							762 ($2\nu_{10}$)				
	ν_{11}	647	646			646.5							678
	ν_{12}								383 ($2\nu_{12}$)				
b_2	ν_{13}	2372											
	ν_{14}	2209	2209										
	ν_{15}	1387	1062										
	ν_{16}	1062	1007										
	ν_{17}	900	1263										
	ν_{18}	689											

The following procedure, workup, and purification were carried out in the dark. Allyl-2-d_1 alcohol (1.0 g, 16.9 mmol) and methyltriphenoxyphosphonium iodide (9.95 g, 22.0 mmol) were combined in 25 mL of diethyl ether at room temperature and stirred under Ar for 44 h. The reaction mixture was then washed with saturated, aqueous sodium thiosulfate and saturated aqueous sodium chloride. The aqueous layers were extracted three times with diethyl ether and the combined ether layers were dried over magnesium sulfate. Ether was distilled off at atmospheric pressure with gentle heating. When the solvent level became low, all of the volatile components were removed by distillation under reduced pressure, leaving a viscous orange residue behind. The volatile components were then placed in the smallest flask possible, and all remaining ether was distilled under atmospheric pressure. The allyl iodide was then distilled under aspirator vacuum, yielding 1.54 g (54% yield) of a light yellow oil. The product $CH_2{=}CDCH_2I$ is 95% pure, with methyl iodide being the primary contaminant. The allyl iodide was stored in a freezer over copper metal for stability. The product is heat and light sensitive. ^{1}H NMR (200 MHz, $CDCl_3$) δ 3.87 (s), 4.98 (m), 5.24 (m). ^{2}H NMR (61.47 MHz, C_6H_6, referenced to C_6D_6) δ 5.66. ^{13}C NMR (100 MHz, C_6D_6) δ 5.47 (s), 117.51 (s), 135.98 (t).

Allyl-d_5 iodide was prepared from allyl-d_5 alcohol (Aldrich) in the same manner as allyl-2-d_1 iodide (56% yield). Gas chromatographic analysis shows the product $CD_2{=}CDCD_2I$ to be 94% pure. ^{1}H NMR (400 MHz) shows methyl iodide as the primary contaminant, along with minor amounts of nondeuterated allyl iodide, diethyl ether, and phenol. ^{2}H NMR (61.47 MHz, C_6H_6, referenced to C_6D_6) δ 3.22, 4.53, 4.72, 5.63. ^{13}C NMR (100 MHz, C_6D_6) δ 5.21 (m), 116.93 (m), 135.58 (t).

D. Computational Methods. The vibrational lines in this work were assigned using harmonic frequencies from electronic structure calculations as a guide. We used the density functional method of Becke,[20,21] UB3LYP with a 6-311-G (p,d) basis set and the Gaussian 98[22] computational suite to calculate harmonic frequencies of allyl radical and its isotopomers. These computational values for allyl radical are listed in Table 2.

III. Results and Discussion

A. PIMS Optimization of the Allyl Radical Source. Prior to spectroscopic analysis of allyl radical, pyrolysis conditions were established for the precursors. The bond enthalpies of the possible precursors are all known:[3,23,24] $DH_{298}(CH_2CHCH_2{-}Br) = 251 \pm 5$ kJ mol^{-1} [60.0 ± 1.1 kcal mol^{-1}], $DH_{298}(CH_2{-}CHCH_2{-}I) = 200 \pm 4$ kJ mol^{-1} [47.7 ± 1.0 kcal mol^{-1}], and $DH_{298}(CH_2CHCH_2{-}CH_2CHCH_2) = 285 \pm 4$ kJ mol^{-1} [68.1 ± 1.0 kcal mol^{-1}]. Allyl iodide was found to be the best precursor; PIMS traces of the $CH_2{=}CHCH_2I$ are shown in

TABLE 2: Calculated UB3LYP/6-311 G(p,d) Harmonic Frequencies (ω/cm^{-1}) and Infrared Intensities (A/km mol^{-1}) for the $\tilde{X}$ $^2A_2$ Allyl Radical (All Values Unscaled). To View the Animated Vibrational Modes, See http://ellison.colorado.edu/allyl

			CH_2CHCH_2		CH_2CDCH_2		CD_2CDCD_2	
ω		local mode description	ω/cm^{-1}	A/km mol^{-1}	ω/cm^{-1}	A/km mol^{-1}	ω/cm^{-1}	A/km mol^{-1}
1	a_1	CH_2CHCH_2 asymmetric CH_2 st	3235	21.0	3233	16.8	2410	11.2
2		CH_2CHCH_2 symmetric CH_2 st	3141	4.6	3140	7.4	2316	2.9
3		CH_2(C−H)CH_2 stetch	3128	15.8	2311	8.9	2278	7.7
4		symmetric CH_2 scissors	1517	2.9	1514	2.8	1291	0.3
5		CH_2−CH−CH_2 stretch + CH_2 scis	1270	0.9	1246	1.1	1040	1.4
6		CH_2−CH−CH_2 stretch +CH_2 rock	1037	0.1	1036	0.1	856	0.3
7		CH_2−CH−CH_2 bend	429	0.0	425	0.0	350	0.0
8	a_2	CH_2CHCH_2 out-of-phase umbrella	786	0.0	786	0.0	622	0.0
9		CH_2−CH−CH_2 out-of-phase twist	553	0.0	553	0.0	393	0.0
10	b_1	CH_2(C−H)CH_2 out-of-plane bend	1014	21.4	816	9.0	784	1.4
11		CH_2CHCH_2 in-phase umbrella	811	78.0	808	80.0	657	52.0
12		CH_2−CH−CH_2 in-phase twist	532	16.5	531	17.0	408	12.5
13	b_2	CH_2CHCH_2 asymmetric CH_2 stretch	3232	5.8	3232	3.1	2408	3.0
14		CH_2CHCH_2 symmetric CH_2 stretch	3134	8.7	3134	4.3	2273	4.2
15		asymmetric CH/CH_2 scissors	1511	1.0	1494	0.6	1375	0.0
16		asymmetric CH_2−CH−CH_2 stretch + CH/CH_2 scissors	1423	6.7	1348	3.5	1075	4.4
17		asymmetric CH_2−CH−CH_2 stretch + CH bend	1207	0.3	1036	1.5	939	0.1
18		asymmetric CH/CH_2 rock	936	0.0	851	0.0	699	0.1

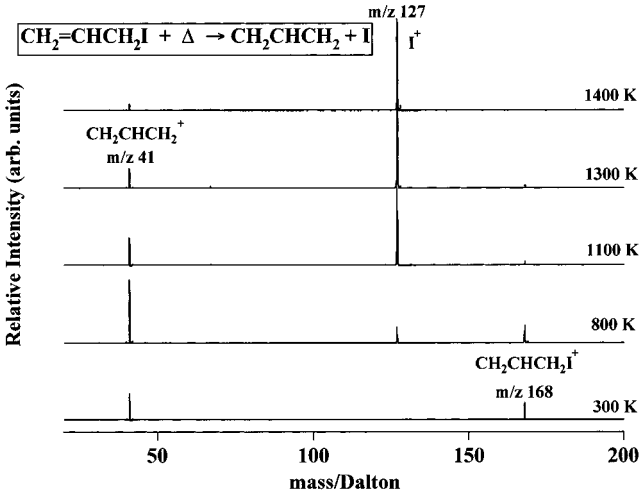

Figure 1. Photoionization mass spectra of the output of the hyperthermal nozzle. The nozzle temperature varies from 300 to 1400 K. The molecular beam is photoionized by 118.2 nm laser light (10.487 eV), and the ions are anaylzed with a reflectron TOF mass spectrometer. The appearance of I^+ at a nozzle temperature of 1100 K shows the threshold for the thermal dissociation: CH_2=$CHCH_2I$ + 1100 K → CH_2CHCH_2 + I.

Figure 1 and demonstrates that the parent ion, $[CH_2$=$CHCH_2I]^+$, undergoes a large amount of photoionization fragmentation: $CH_2CHCH_2I^+ \rightarrow CH_2CHCH_2^+ + I$. The simultaneous presence of I^+ and $CH_2CHCH_2^+$ is a clear signal that we are pyrolyzing CH_2=$CHCH_2I$ and producing allyl radicals. On the basis of this figure, we opted to dose at 1150 K, where CH_2=C=CH_2 production is minimal and to subtract the allyl iodide precursor spectra from the final spectra shown in this work.

B. Vibrational Spectroscopy of Allyl Radical. High-resolution, gas-phase studies of the infrared absorption spectrum of the CH_2CHCH_2 radical have been reported. Allyl radicals were studied using high-resolution IR absorption techniques[25,26] in a cooled jet. In these works the in-phase and out-of-phase asymmetric C−H stretches ν_1 (3113.98488 cm^{-1}) and ν_{13} (3110.59857 cm^{-1}) were detected with rotational resolution. The C_{2v} symmetry of the allyl radical was also confirmed by studying the nuclear spin statistics in rotationally resolved spectra. Hirota[27] studied ν_{11}, the most intense vibration in allyl radical. The lines in the ν_{11} rotationally resolved manifold were fitted using a vibration−rotation Hamiltonian and this fundamental was shown to be polarized along the molecular *c*-axis and to be a b_1 transition. The rotational constants were used to calculate C−C bond lengths of 1.3869 ± 0.0033 Å and the CCC angle of 123.96 ± 0.48° . The change in the centrifugal distortion constants induced by the coupling of ν_{11} and ν_7 in allyl radical has also been described.[28]

Earlier EPR measurements indicated that allyl radical contains only 3 types of hydrogens.[29,30] This is consistent with CH_2-$CHCH_2$ being planar and having C_{2v} symmetry. Equation 2 shows the allyl radical's symmetry axis; the *x* axis is out of the plane and defines the B_1 symmetry axis or the molecular *c* axis.

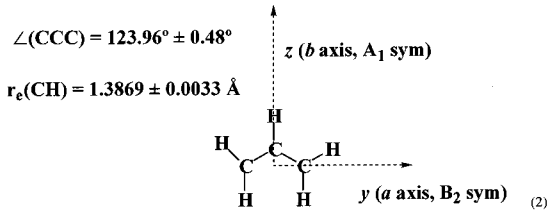

The ground electronic state of the allyl radical is ($\tilde{X}$) $^2A_2$, and this molecule has 18 vibrational modes. The irreducible representations of the allylic modes are: $\Gamma_{VIB}(CH_2CHCH_2)$ = 7 a_1 ⊕ 2 a_2 ⊕ 3 b_1 ⊕ 6 b_2. The two a_2 modes are not IR active so an infrared study should only find 16 separate fundamentals.

The negative ion photoelectron spectrum[9,10] of the allylic anion has been observed; $CH_2CHCH_2^- + \hbar\omega_0 \rightarrow CH_2CHCH_2 + e^-$. Vibrational progressions observed in the spectrum correspond to the a_1 modes ν_6, the CCC stretch, and ν_7 the CCC bend. The overtone of the nontotally symmetric b_1 mode ν_{11} was (weakly) observed as well. A number of multiphoton ionization (MPI) studies[31−34] investigated the $\tilde{B}$ $^2A_1 \leftarrow \tilde{X}$ $^2A_2$ transition in the 3s Rydberg state of CH_2CHCH_2. In these studies Sappey et al.[34] used electronic structure calculations to assign vibrational modes ν_7, ν_{12}, and ν_9 of the ground-state CH_2-$CHCH_2$, $\tilde{X}$ $^2A_2$. Minsek et al.[33] used rotational contours to fit their MPI data and re-assigned these same modes. From the resonance Raman spectra of Getty et al.[35−37] and Liu et al.,[38] many of the totally symmetric modes of allyl radical and allyl-d_5 were assigned. In Raman studies the most intense lines in the Stokes spectrum are attributed to totally symmetric vibrations. Even overtones of nontotally symmetric vibrations, which reflect large changes between the excited-state geometry and the ground-state such as ν_9, ν_{10}, and ν_{12}, were also detected.

The CH_2CHCH_2 radical has been the subject of several previous matrix IR studies.[39−43] Many of the vibrational modes in these studies are consistent with modes identified in the present work. Allyl radical lines were confirmed through performing annealing experiments where the matrices were heated to temperature of 30−40 K. Lines that were depleted were believed to be due to allyl radical. In these earlier studies, the best ab initio electronic structure calculations (at that time) were used as a guide for assignments. There were no mechanisms to assign symmetries of the separate vibrational modes.

All of the previous experimental spectroscopic work on the CH_2CHCH_2 radical is summarized in Table 1.

C. Electronic Structure of Allyl Radical and Photoorientation Experiments. To anticipate the later photoorientation experiments, the electronic structure of allyl radical is reviewed.[1,3] The electronic configuration of the ground state is $...(1b_1)^2(1a_2)^1$ leading to a $\tilde{X}\ ^2A_2$ symmetry. In a first-order approximation, the first low-lying excited electronic state of CH_2CHCH_2 will be a superposition of the two configurations, $(1b_1)^1(1a_2)^2$ and $(1b_1)^2(2b_1)^1$, leading to $^2B_1$ symmetry for the $\tilde{A}$ CH_2CHCH_2 state.

The electronic spectrum of allyl radical was first detected by Currie and Ramsey[44] who studied the lower electronic transition, $\tilde{A} \leftarrow \tilde{X}$, centered at 408.3 nm. From the diffuseness of the band of the transitions and lack of rotational structure they concluded that allyl radical predissociates in the lowest excited state. Callear and Lee[45] studied the upper excited states of allyl radical in the 210−250 nm region. They assigned their observed spectrum to transitions in an upper state of $^2B_1$ symmetry. These studies were confirmed by Maier[41] who also observed a strong structureless UV transition centered at 213 nm and a weak transition centered at 408.5 nm indicating that the allyl radical dissociates in both excited-state manifolds. The upper excited-state potential energy surface was calculated by Ha et al.[46] and subsequently investigated using MPI by Blush et al.[47] Blush studied the $\tilde{D}\ ^2B_2 \leftarrow \tilde{X}\ ^2A_2$, $\tilde{C}\ ^2B_1 \leftarrow \tilde{X}\ ^2A_2$, and the dipole-forbidden, $\tilde{B}\ ^2A_1 \leftarrow \tilde{X}\ ^2A_2$, transitions in the 238−250 nm region. They found substantial vibronic mixing between electronic levels in the excited-state manifold. They further conjecture that allyl radical loses its C_{2v} symmetry in making the forbidden $\tilde{B}\ ^2A_1 \leftarrow \tilde{X}\ ^2A_2$ transition allowed.

In photoorientation experiments we excite a dissociative electronic transition of CH_2CHCH_2 with known symmetry in order to selectively deplete the matrix-isolated allyl species and generate a preferentially aligned distribution of radicals. We use the polarized 351 nm line from an Ar II laser to excite the blue edge of the $\tilde{A}\ ^2B_1 \leftarrow \tilde{X}\ ^2A_2$ transition. For the allyl transition dipole moment, $\langle ^2B_1|\hat{\mu}|^2A_2\rangle$, to be nonzero, the $\tilde{A}\ ^2B_1 \leftarrow \tilde{X}\ ^2A_2$ transition must be polarized along μ_y (or B_2) and is aligned parallel to the main *a* molecular axis of allyl radical, see eq 2.

When the matrix is dosed the cryogenically trapped CH_2CHCH_2 radicals have a random distribution. Irradiation of these allyl radicals with polarized UV light at 351 nm dissociates molecules that have a substantial projection of their transition dipole moments parallel to the depleting laser light.[48] The probability of photon absorption and subsequent dissociation for a molecule *i* is proportional to $\langle \cos^2(\theta_i)\rangle$ where θ_i is the angle between the transition dipole moment $\hat{\mu}_i$ and **E**. The molecules remaining after the photodepletion process have their transition moments $\hat{\mu}_i$ preferentially oriented perpendicular with respect to the **E** vector of the depleting laser light.

This preferentially oriented ensemble of radicals is prepared using laser light, which is horizontally oriented with respect to the laboratory frame or in the Z direction. The allyl molecules are preferentially oriented with their molecular *a* axes perpendicular to this depleting laser light and thus vertically oriented with respect to the laboratory frame. The ensemble of molecules are then measured using two linearly independent polarized IR beams in the *Z* and *Y* directions, parallel and perpendicular to the depleting laser light. The IR absorption intensity for the a_1 (parallel to molecular *b* axis) and the b_1 modes (parallel to the molecular *c* axis) will be greater using IR light polarized in the *Z* direction and be less using IR light polarized in the *Y* direction. That is $I_Z - I_Y > 0$ (exhibit positive linear dichroism or LD) for modes of a_1 and b_1 symmetry. Correspondingly absorption intensities for b_2 modes will be lower using horizontally oriented (*Z* direction) IR light for measurement; that is $I_Z - I_Y < 0$ (exhibit negative linear dichroism or LD) for modes of b_2 symmetry. In this work the symmetry of the b_2 modes is determined unambiguously. Unfortunately, because the excited state manifold has a high degree of mixing, there is no convenient method to preferentially orient the ensemble of trapped allyl radicals in order to separately assign the a_1 and b_1 modes.

D. Assignments of the Allyl Radical IR Spectra. Matrix-isolated allyl radicals are reactive. Three contaminants that we repeatedly encounter in this work are allene, propene, and 1,5-hexadiene. The sequential bond enthalpies of the allyl radicals are known.[4]

$$CH_2{=}CHCH_3 \rightarrow CH_2CHCH_2 + H \qquad DH_{298} = 372 \pm 2 \text{ kJ mol}^{-1} \quad (3a)$$

$$CH_2CHCH_2 \rightarrow CH_2{=}C{=}CH_2 + H \qquad DH_{298} = 109 \pm 3 \text{ kJ mol}^{-1} \quad (3b)$$

Consequently a pair of allyl radicals can disproportionate in a 263 kJ mol^{-1} (62.7 ± 0.7 kcal mol^{-1}) exothermic process: $CH_2CHCH_2 + CH_2CHCH_2 \rightarrow CH_2{=}C{=}CH_2 + CH_3CH{=}CH_2$. Likewise a pair of allyl radicals can simply dimerize in a 285 kJ mol^{-1} (68.1 ± 1.0 kcal mol^{-1}) exothermic process to produce $CH_2{=}CHCH_2{-}CH_2CH{=}CH_2$. Peaks marked as $CH_2{=}C{=}CH_2$ are the most intense bands of allene,[49−51] $\nu_6(CH_2{=}C{=}CH_2) = 1957$ cm^{-1} and $\nu_{10}(CH_2{=}C{=}CH_2) = 837$ cm^{-1}. The feature marked with **H** in the parent allyl radical spectra at 914 cm^{-1} (Figure 2) is the most intense band of 1,5-hexadiene, the allyl-allyl recombination product. Smaller peaks (not marked) attributed to 1,5-hexadiene are found at 996 and 1361 cm^{-1}.

We have measured the infrared absorption spectrum of three C_{2v} isotopomers of the allyl radical: allyl-d_0 (CH_2CHCH_2), allyl-d_1 (CH_2CDCH_2), and allyl-d_5 (CD_2CDCD_2). The results are displayed in Figures 2−13. The final experimental vibrational frequencies for the matrix-isolated allyl radicals are collected together in Table 3.

Figure 2 is an overview of the entire infrared absorption spectrum of the parent allyl radical, CH_2CHCH_2, $\tilde{X}\ ^2A_2$. The experimental IR spectrum is the black trace and each of the assigned allyl radical fundamentals is marked by a bullet (•). Colored red and offset above the IR absorption spectrum are the DFT calculated harmonic predictions $\{\omega\}_i$ [UB3LYP/6-311-G(d, p)] from Table 2. In the construction of Figure 2, we have ignored the two IR inactive harmonic modes, ω_8 and ω_9, and only plotted the active modes in order for an uncluttered comparison with our experiment. The lowest frequency CCC bending a_1 mode ω_7 is not shown because it is predicted to appear at 429 cm^{-1}, below the range of our MCT detector. The irreducible representations of allyl radical's vibrations are:

TABLE 3: Experimental Vibrational Frequencies (ν/cm^{-1}) and Relative Infrared Intensities (A/km mol^{-1} as a Percent of the Base Peak) for the Matrix-Isolated $\tilde{X}\ ^2A_2$ Allyl Radical[a]

			CH_2CHCH_2			CH_2CDCH_2			CD_2CDCD_2		
ν		local mode description	ν/cm^{-1}	A/%	polarity	ν/cm^{-1}	A/%	polarity	ν/cm^{-1}	A/%	polarity
1	a_1	CH_2CHCH_2 asymmetric CH_2 st	3109	18	+	3106	38	+			
2		CH_2CHCH_2 symmetric C CH_2 stretch	3052	5	+	3022	4		2285	4	+
3		$CH_2(C-H)CH_2$ stretch	3027	2	+	2268	8	+	2215	4	+
4		symmetric CH_2 scissors	1478	6	+	1474	15	+	1263		
5		$CH_2-CH-CH_2$ stretch + CH_2 scissors	1242	1	+	1220	4	+	1018	4	+
6		$CH_2-CH-CH_2$ stretch + CH_2 rock	na			1012	3	+	844	1	
7		$CH_2-CH-CH_2$ bend	na			na			na		
8	a_2	CH_2CHCH_2 out-of-phase umbrella	775 ?			na			na		
9		$CH_2-CH-CH_2$ out- of-phase twist	na			na			na		
10	b_1	$CH_2(C-H)CH_2$ out-of-plane bend	983	22	+	802	141	+	767	3	
11		CH_2CHCH_2 in-phase umbrella	801	100	+	787	100	+	647	100	+
12		$CH_2-CH-CH_2$ in-phase twist	510	14	+	511	22	+			
13	b_2	CH_2CHCH_2 asymmetric CH_2 stretch	3107	4	−	3106	20	−	2372	2	−
14		CH_2CHCH_2 symmetric CH_2 st	3020	3	−	3013	7	−	2209	6	−
15		asymmetric CH/CH_2 scissors	1464	17	−	1452	22	−	1387	13	−
16		asymmetric $CH_2-CH-CH_2$ stretch + CH/CH_2 scissors	1390	1	−	1352	5	−	1062	7	−
17		asymmetric $CH_2-CH-CH_2$ stretch ⊕ CH bend	1182		−	1010	1		900	7	−
18		asymmetric CH/CH_2 rock	na			845			689		

[a] See Figures 2−13 for details. Na means not available.

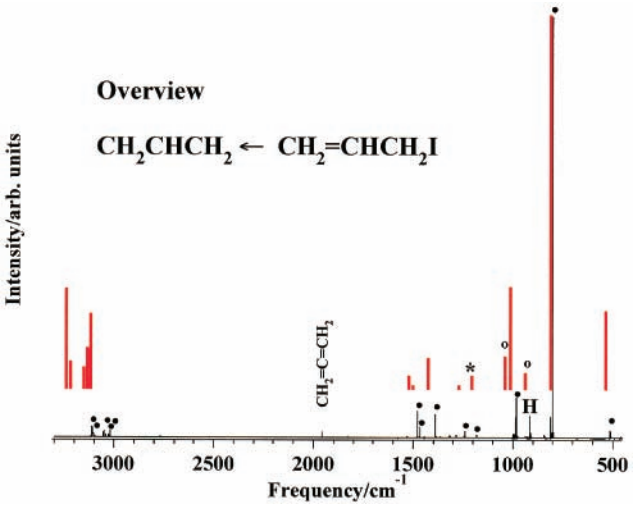

Figure 2. An overview of the infrared absorption spectrum of matrix isolated allyl radical. Allyl radicals are produced by the dissociation of CH_2═$CHCH_2I$ in a hyperthermal nozzle at 1150 K. The solid, black trace is the experimental IR spectrum and the fundamental infrared modes {ν} are marked by bullets (•). The DFT calculated [UB3LYP/6-311-G(d,p)] harmonic frequencies {ω} are plotted as red sticks. Several of the harmonic modes are predicted to be very weak and have been scaled by a factor of 10 and are marked by a star (∗); weak ω modes scaled by 100 are marked by ( ).

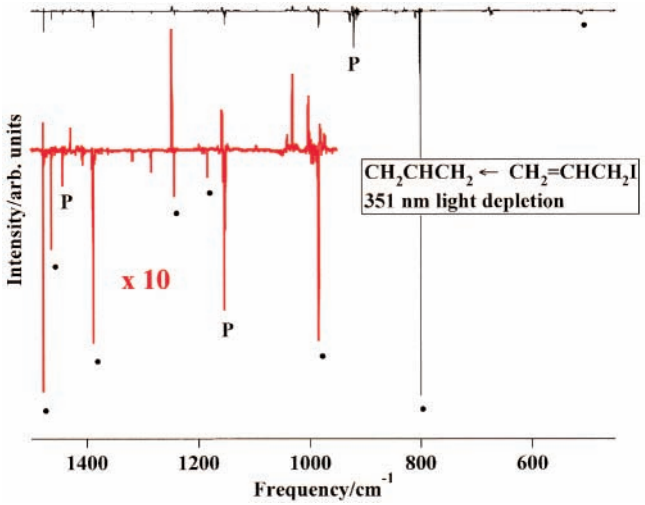

Figure 3. An infrared spectrum showing the depletion of matrix isolated CH_2CHCH_2 radicals "fingerprint region" upon bombardment by 351 nm laser light. Excitation of the $\tilde{A}$ state of CH_2CHCH_2 is known to dissociate the radical. Infrared fundamentals of the CH_2CHCH_2 radical are marked by bullets (•). The weak portion of the spectrum between 950 − 1450 cm^{-1} has been scaled by a factor of 10 and is plotted in red. An intense absorption of the allyl radical precursor, CH_2═$CHCH_2I$, is marked by **P**.

$\Gamma_{VIB}(CH_2CHCH_2) = 7\ a_1 \oplus 2\ a_2 \oplus 3\ b_1 \oplus 6\ b_2$. Consequently there are 15 red peaks marked on the spectrum in Figure 2 (18 modes of CH_2CHCH_2, less the 2 a_2 modes, less the low-frequency a_1 mode ω_7). Three of the harmonic modes (ω_5, ω_6, and ω_{17}) are predicted to be very weak ($A_i \leq 0.1$ km mol^{-1}) and will be difficult to detect. Consequently we have scaled these three modes by factors of 10 (marked with a star, *) and 100 (marked with a **o**) in Figure 2.

Qualitatively the comparison of the predicted harmonic modes and our experimental spectrum in Figure 2 is quite good. All the harmonic frequencies are predicted close to our assigned fundamentals although the computed harmonic infrared intensities are very erratic.

A matrix of allyl radicals was depleted by irradiation at 351 nm, exciting the blue edge of the (dissociative) $\tilde{A}\ ^2B_1 \leftarrow \tilde{X}\ ^2A_2$ transition. Several sharp features are depleted in the IR spectrum and are likely part of the CH_2CHCH_2 spectrum; these depletions are marked with a bullet (•) in Figure 3. The weak portion of Figure 3 between 1000 and 1400 cm^{-1} has been expanded (in red) by a factor of 10 to clearly show the CH_2CHCH_2 depletions.

Excitation with a polarized laser at 351 nm produces a linear dichroism spectrum ($I_Z - I_Y$) of allyl, Figure 4. The negatively polarized features must have b_2 symmetry (vide supra) while the positive peaks can be polarized either a_1 or b_1. With reference to the harmonic frequencies of Figure 2 and Table 2 and by matching the depletion and polarization spectra, we have assigned the CH_2CHCH_2 vibrations in Figure 4. There are five features that have negative polarization. The bands at 1152 and 920 cm^{-1} are strong features of CH_2═$CHCH_2I$ and marked as **P** (for precursor). The negatively polarized bands at 1464, 1390, and 1182 cm^{-1} are assigned as b_2 fundamentals (ν_{15}, ν_{16}, and ν_{17}). Since the linear dichroism spectra cannot distinguish between the a_1 and b_1 modes, we must rely on the computed

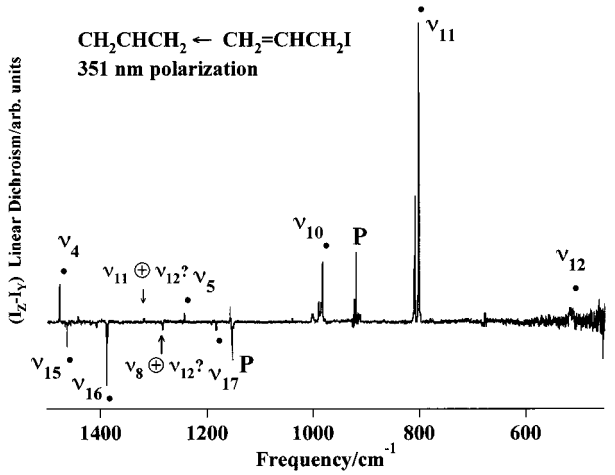

Figure 4. A linear dichroism spectrum of the CH_2CHCH_2 radical following matrix-depletion by polarized 351 nm light. IR bands of CH_2-$CHCH_2$ that are b_2 polarized will have a negative dichroism while IR features with a_1 and b_1 polarization will have a positive dichroism. Two weak features are attributed to combination bands of ν_{12} of allyl radical; these are marked by $(\nu_{11} \oplus \nu_{12})$ and $(\nu_8 \oplus \nu_{12})$. These absorptions are more clearly evident in Figure 5. Allyl fundamentals are marked by a bullet (•), while **P** is a precursor band.

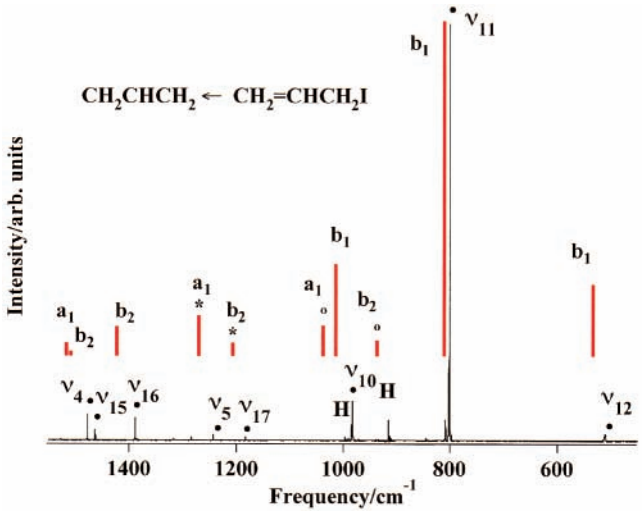

Figure 5. A final comparison of allyl radical's fingerprint region. The DFT harmonic frequencies $\{\omega\}$ in red reproduce the experimental fundamentals $\{\nu\}$ marked by bullets (•). The intensities (∗) of the harmonic modes, ω_5 and ω_{17}, have been scaled by a factor of 10. Two of the harmonic modes, ω_6 and ω_{18}, are exceptionally weak and have had their intensities ( ) scaled by a factor of 100. We could not observe these two fundamentals, ν_6 and ν_{18}.

harmonic frequencies in Table 2 to assign the spectra in Figure 4. The two bands at 1478 and 1242 cm^{-1} are assigned as a_1 modes (ν_4 and ν_5) but the features at 983, 801, and 510 cm^{-1} are clearly b_1 modes (ν_{10}, ν_{11}, and ν_{12}). We conjecture that the weak band at 1317 cm^{-1} is likely a combination band, $(\nu_{11} \oplus \nu_{12})$. Such a transition would be polarized $(b_1 \otimes b_1)$ or a_1 which is compatible with the LD spectrum, Figure 4. The weak, negatively polarized feature at 1285 cm^{-1} could be possibly be a combination band of $(\nu_8 \oplus \nu_{12})$. Such a band would be polarized $(a_2 \otimes b_1)$ or b_2 with a negatively polarized absorption in Figure 4. This implies an assignment of 775 cm^{-1} for the a_2 mode ν_8, which has never been assigned before. The predicted harmonic mode ω_8 from Table 2 is 786 cm^{-1}. Figure 5 is a summary of the entire fingerprint region of the CH_2CHCH_2 radical; this figure is a color-coded comparison of our experimental spectra (in black) and the red sticks which locate the

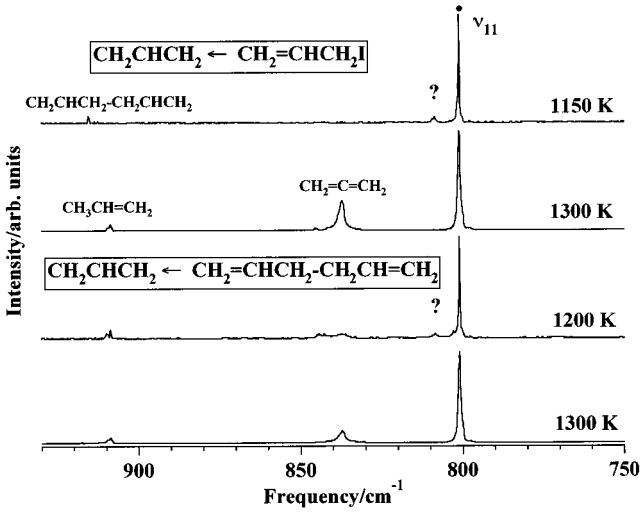

Figure 6. The feature at 809 cm^{-1} in Figures 2−4 is not a fundamental of allyl radical. This band appears in matrices produced by thermal dissociation (1150 K) of $CH_2{=}CHCH_2I$ or $CH_2{=}CHCH_2{-}CH_2CH{=}CH_2$. If the hyperthermal nozzle is heated to higher temperatures (1300 K), the 809 cm^{-1} feature disappears and signals from the radical/radical disproportionation appear ($CH_2{=}C{=}CH_2$ and $CH_2{=}CHCH_3$). However the allyl fundamental at 801 cm^{-1} (ν_{11}) persists.

harmonic frequencies. The experimental values are collected together in Table 3. In so far as we can measure, the ordering of the harmonic frequencies, $\{\omega\}$ in red, match our experimental assignments exactly. We cannot detect the CH_2CHCH_2 modes ν_6 and ν_{18} which are predicted (Table 2) to be extremely weak. There are two absorptions in the fingerprint region that clearly belong to $CH_2{=}CHCH_2{-}CH_2CH{=}CH_2$ (**H**).

There is an intense feature near at 809 cm^{-1} near ν_{11} in Figure 4. Because this line has been consistently measured in many allyl radical studies, we believe that it must be attributed to either the CH_2CHCH_2 radical or species associated with it. Although we could not determine the carrier of the 809 cm^{-1} line, we believe that it is not a CH_2CHCH_2 radical fundamental nor combination band as has been suggested in earlier studies. We produced CH_2CHCH_2 radical from both $CH_2{=}CHCH_2I$ at 1150 and 1300 K and from $CH_2{=}CHCH_2{-}CH_2CH{=}CH_2$ at 1200 and 1300 K. Spectra of the region are shown in Figure 6. In the higher temperature production of CH_2CHCH_2 radical, the 809 cm^{-1} is no longer present although other allyl radical features persist. IR signals of the disproportionation products, $CH_3CH{=}CH_2$ and $CH_2{=}C{=}CH_2$, are clearly identified. This 809 cm^{-1} is present in both lower temperature spectra. Also note that the 809 cm^{-1} has a dramatically different intensity pattern in polarization spectrum in Figure 4 than it had in the depletion spectrum in Figure 3. In earlier studies, researchers produced CH_2CHCH_2 radical in low-pressure pyrolysis at 1100 to 1200 K only. We believe that this line is a mode of some intermediate species in the thermal production of CH_2CHCH_2 radical.

Figure 7 shows the depletion of the CH portion of the IR spectrum of CH_2CHCH_2. We expect to find 5 CH absorption features and Figure 7 clearly shows five bands. The (eventual) fundamentals are shown as bullets (•). Figure 8 is the LD spectrum of allyl that results from polarization of the matrix with 351 nm light. By symmetry we know that the five CH stretches transform like $(3\ a_1 \oplus 2\ b_2)$ modes. Consequently we assign the three a_1 CH stretches ν_1, ν_2, and ν_3 (see Table 3). Earlier high-resolution IR absorption studies[25,26] of the highest (a_1, b_2) CH stretching pair, ν_1 and ν_{13}, have observed these features at 3113.98488 ± 0.00089 cm^{-1} and 3110.59857 ±

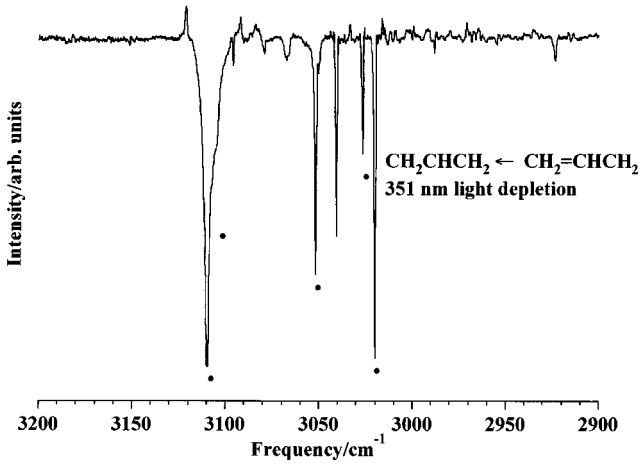

Figure 7. An infrared spectrum showing the depletion of matrix isolated CH_2CHCH_2 radicals "CH region" upon bombardment by 351 nm laser light. Infrared fundamentals of the CH_2CHCH_2 radical are marked by bullets (•).

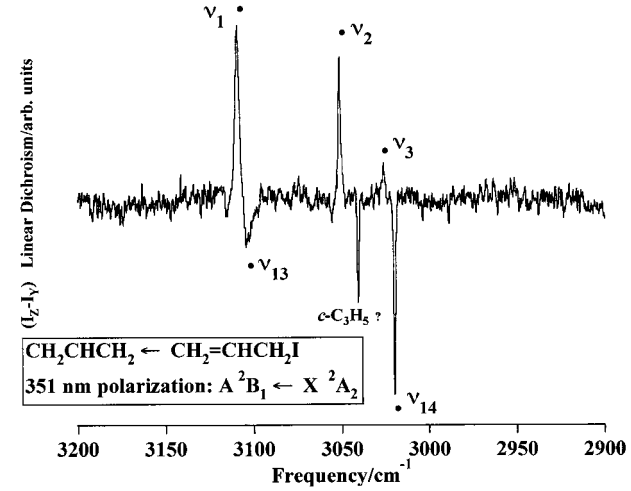

Figure 8. A linear dichroism spectrum of the CH_2CHCH_2 radical following matrix-depletion by polarized 351 nm light. IR bands of CH_2-$CHCH_2$ that are b_2 polarized will have a negative dichroism while IR features with a_1 and b_1 polarization will have a positive dichroism. Allyl fundamentals are marked by a bullet (•); the strong feature at 3040 cm^{-1} is not an allyl radical mode.

0.00036 cm^{-1}, respectively (see Table 1). Rotational analysis clearly established that ν_1 is a *b*-type band consistent with an a_1 transition while ν_{13} is an *a*-type band or b_2 mode. The harmonic frequencies (Table 2) predict the (ω_1, ω_{13}) pair at 3235 and 3232 cm^{-1}. Consequently we assign the first two matrix bands in Figure 8 as $\nu_1 = 3109$ cm^{-1} and $\nu_{13} = 3107$ cm^{-1}. We have now assigned all of the CH stretches but for ν_{14}. We appeal to the predicted harmonic frequencies in Table 2 where ω_{14} is estimated to be 3134 cm^{-1}; consequently we assign the intense, negatively polarized band at 3020 cm^{-1} as ν_{14}. This leaves us with the strong, negatively polarized feature at 3040 cm^{-1} in Figure 8.

The line at 3040 cm^{-1} is not consistent with being a combination band of allyl radical fundamentals. There are no combinations of two fundamentals which result in a mode at 3040 cm^{-1} and that would exhibit b_2 type LD. Yet this line is consistently found all matrix CH_2CHCH_2 radical spectra. Consequently we consider an isomer of CH_2CHCH_2 radical, the cyclopropyl radical (c-C_3H_5). We conjecture that this mode is one of the most intense a″ modes of the c-C_3H_5 radical, ν_{12}. Recently Davis[52] studied the high-resolution IR absorption

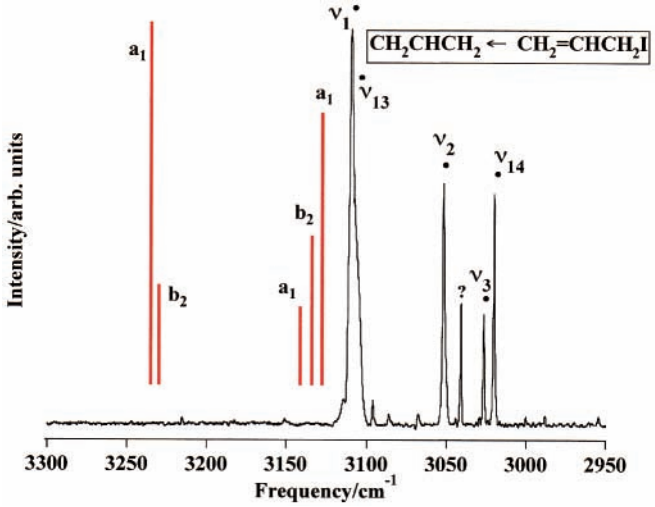

Figure 9. A final comparison of allyl radical's CH stretching region. The DFT harmonic frequencies {ω} in red reproduce the experimental fundamentals {ν} marked by bullets (•).

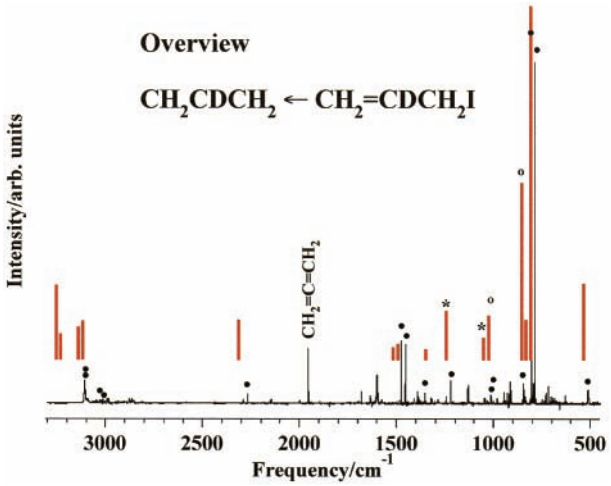

Figure 10. An overview of the infrared absorption spectrum of matrix isolated allyl radical. Allyl radicals are produced by the dissociation of CH_2═$CDCH_2I$ in a hyperthermal nozzle at 1150 K. The solid, black trace is the experimental IR spectrum and the fundamental infrared modes {ν} are marked by bullets (•). The DFT calculated [UB3LYP/6-311-G(d,p)] harmonic frequencies {ω} are plotted as red sticks. Several of the harmonic modes are predicted to be very weak and have been scaled by a factor of 10; these weak {ω} transitions are marked by a star (∗). Two harmonic modes are exceptionally weak and have been scaled by a factor of 100 are marked by ().

spectra of a pulsed electric discharge of cyclopropyl bromide wherein he observed a cyclopropyl C−H stretch at 3040.8458 cm^{-1}; this he identified as a *c*-type band or a″ mode. Our unassigned matrix band is also at 3040 cm^{-1} and this is a significantly smaller gas-to-matrix shift than the 4 or 5 cm^{-1} shift that has been observed for allyl radical C−H stretches. However, different species could certainly have different shifts.

Figure 9 is a direct comparison of the UB3LYP/6−311-G(d,p) harmonic modes (red sticks) with our assigned CH fundamentals for CH_2CHCH_2. The harmonic predictions are very close to our experimental findings except for the (ν_2, ν_3, and ν_{14}) order.

In addition to the parent allyl radical, we have studied its d_1 isotopomer, CH_2CDCH_2, and the d_5 isotopomer, CD_2CDCD_2. Figure 10 is a overview of the CH_2CDCH_2 infrared absorption spectrum. The black trace is the experimental spectrum and the assigned fundamentals are marked by bullets (•). The red sticks are the harmonic frequencies that result from a UB3LYP/6-

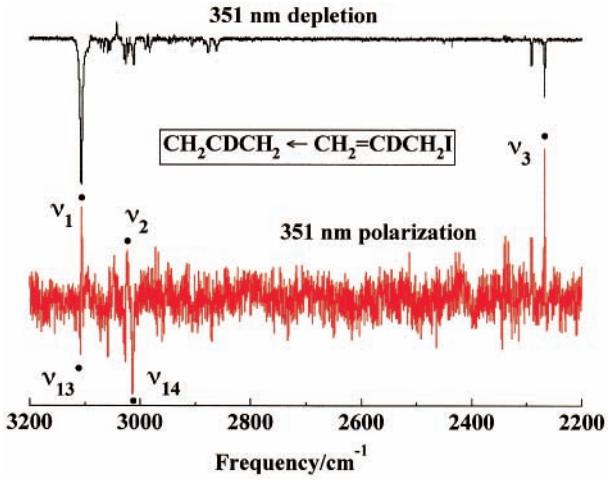

Figure 11. An overplot of the 351 nm depletion spectrum of matrix isolated CH_2CDCH_2 radical (black, on top) with the linear dichroism spectrum (red, on bottom). The CH_2CDCH_2 fundamentals $\{\nu\}$ are marked by bullets (•).

311-G(d,p) electronic structure calculation. Four of the harmonic frequencies (ω_5, ω_6, ω_{17}, and ω_{18}) have very weak intensities and have been scaled; those bands scaled by a factor of 10 have been marked by an star (∗) while those by a factor of 100 by **()**. The final, assigned CH_2CDCH_2 fundamentals are collected in Table 3.

Figure 11 shows the CH/D stretching region of the d_1 isotopomer. The matrix-isolated CH_2CDCH_2 radical is photodissociated with 351 nm radiation in the top of Figure 11; the depleted fundamentals are marked with bullets (•). To confirm the assignment of these CH_2CDCH_2 fundamentals, the matrix was partially depleted with polarized 351 nm light. The linear dichroism spectrum of the resulting polarized matrix is shown at the bottom of Figure 11. The CH_2CDCH_2 radial has four CH stretches, 2 $a_1 \oplus$ 2 b_2, and one CD stretch of a_1 symmetry. Figure 11 clearly demonstrates the identity of the CH a_1 modes, ν_1 and ν_2, as well as the b_2 pair, ν_{13} and ν_{14}. Simple harmonic reasoning would predict that the $CH_2(C-D)CH_2$ stretching frequency would be shifted to a lower frequency, 3027 $cm^{-1}/\sqrt{2}$ or roughly 2140 cm^{-1}. Figure 11 identifies the CD stretch as the a_1 mode, ν_3, shifted down to 2268 cm^{-1}.

The IR spectrum of the d_5 isotopomer, CD_2CDCD_2, is displayed in Figure 12. The CD stretching modes are assigned in Figure 13. The 351 nm photodepleted CD fundamentals are on the top of Figure 13 while the bottom is the linear dichroism spectrum of a 351 nm polarized matrix sample. We can only identify four of the CD fundamentals. One of the a_1 modes, ν_1, is clearly missing. It is surprising that we cannot observe ν_1 of CD_2CDCD_2 since we compute $\omega_1(CD_2CDCD_2)$ to be a strong band (Table 2).

IV. Conclusions

The set of experimental frequencies for the allyl radical (Table 3) are reasonably reproduced by the UB3LYP/6-311-G(d,p) harmonic frequencies in Table 2. Figures 2, 5, 9, 10, and 12 provide a direct, visual comparison of set of experimental frequencies $\{\nu\}$ with the corresponding harmonic ones $\{\omega\}$. A useful test of the computed $\{\omega\}$ values is to check the predicted isotope shifts. A direct comparison of the experimental frequency shifts of the d_0, d_1, and d_5 isotopomers $\{\Delta\nu\}$ with the corresponding harmonic shifts $\{\Delta\omega\}$ is interesting. For example, Table 3 indicates that the intense, b_1 CH_2 in-phase-twisting mode ν_{11} shifts by 14 cm^{-1} in the d_1 isotopomer [801−787 cm^{-1}]

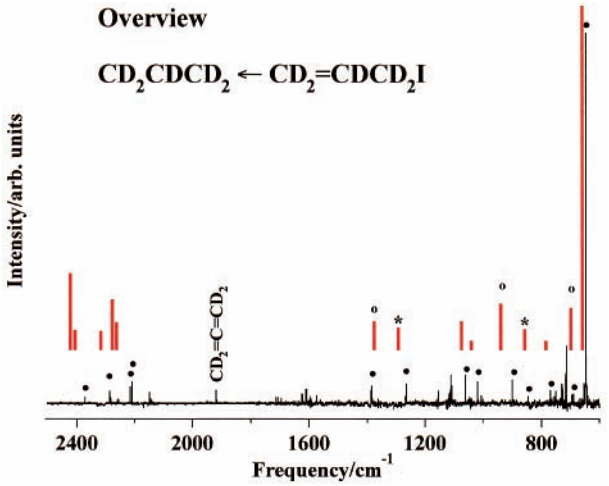

Figure 12. An overview of the infrared absorption spectrum of matrix isolated allyl radical. Allyl radicals are produced by the dissociation of $CD_2{=}CDCD_2I$ in a hyperthermal nozzle at 1150 K. The solid, black trace is the experimental IR spectrum and the fundamental infrared modes $\{\nu\}$ are marked by bullets (•). The DFT calculated [UB3LYP/6−311-G(d,p)] harmonic frequencies $\{\omega\}$ are plotted as red sticks. Several of the harmonic modes are predicted to be very weak and have been scaled by a factor of 10; these weak $\{\omega\}$ transitions are marked by a star (∗). Three harmonic modes are exceptionally weak and have been scaled by a factor of 100 are marked by ().

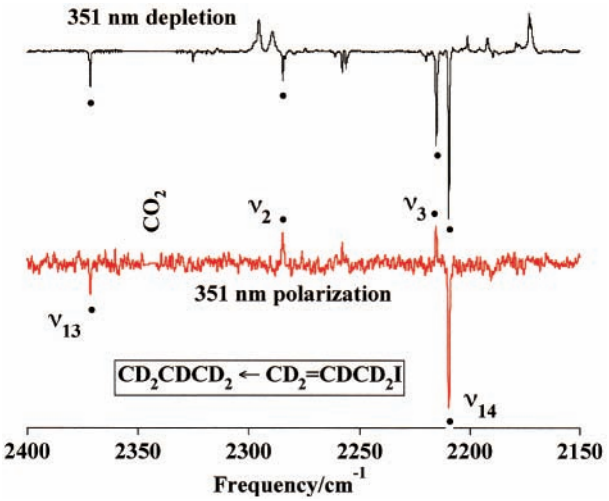

Figure 13. An overplot of the 351 nm depletion spectrum of matrix isolated CD_2CDCD_2 radical (black, on top) with the linear dichroism spectrum (red, on bottom). The CD_2CDCD_2 fundamentals $\{\nu\}$ are marked by bullets (•). The a_1 fundamental of allyl-d_5 ν_1 could not be detected.

and by 154 cm^{-1} in the d_5 isotopomer [801−647 cm^{-1}]; Table 2 indicates that the predicted shifts in ω_{11} are 3 and 154 cm^{-1}, respectively. Table 4 has such a comparison for all of the infrared fundamentals and the results are generally satisfactory. Although the *absolute* harmonic frequencies are off by roughly 2%−4%, Table 4 indicates that the relative isotopic shifts are faithfully reproduced. However the infrared intensities $\{A\}$ for the harmonic modes predicted by UB3LYP/6-311-G(d,p) do not correlate very well with the observed intensities. This may be the fault of the small basis set that we have used to compute $\{\omega\}$.

Before we can make a final recommendation for the gas-phase vibrational frequencies of allyl, we must estimate the magnitude of the gas-to-matrix frequency shifts. Jacox has reviewed the matrix shifts for a large number of diatomic and small polyatomic free radicals and ions trapped in Ne and Ar

TABLE 4: Isotopic Shifts of Allyl Radicals (Tables 2 and 3)

			$\Delta(d_0-d_1)$		$\Delta(d_0-d_5)$	
ν		local mode description	$\{\Delta\nu\}/cm^{-1}$	$\{\Delta\omega\}/cm^{-1}$	$\{\Delta\nu\}/cm^{-1}$	$\{\Delta\omega\}/cm^{-1}$
1	a_1	CH_2CHCH_2 asymmetric CH_2 stretch	3	2		825
2		CH_2CHCH_2 symmetric CH_2 stretch	30	1	767	825
3		$CH_2(C-H)CH_2$ stretch	759	817	812	850
4		symmetric CH_2 scissors	4	3	215	226
5		$CH_2-CH-CH_2$ stretch + CH_2 scissors	22	24	224	230
6		$CH_2-CH-CH_2$ stretch + CH_2 rock		1		181
7		$CH_2-CH-CH_2$ bend		4		79
8	a_2	CH_2CHCH_2 out-of-phase umbrella				
9		$CH_2-CH-CH_2$ out-of-phase twist				
10	b_1	$CH_2(C-H)CH_2$ out-of-plane bend	181	198	216	230
11		CH_2CHCH_2 in-phase umbrella	14	3	154	154
12		$CH_2-CH-CH_2$ in-phase twist	-1	1		124
13	b_2	CH_2CHCH_2 asymmetric CH_2 stretch	1	0	735	824
14		CH_2CHCH_2 symmetric CH_2 stretch	7	0	811	861
15		asymmetric CH/CH_2 scissors	12	17	77	136
16		asymmetric $CH_2-CH-CH_2$ stretch + CH/CH_2 scissors	38	75	328	348
17		asymmetric $CH_2-CH-CH_2$ stretch + CH bend	172	171	282	268
18		asymmetric CH/CH_2 rock		85		237

TABLE 5: Recommended Vibrational Frequencies (ν/cm^{-1}) for $\tilde{X}\ ^2A_2$ Allyl Radical

ν		local mode description	ν/cm^{-1}	ref
1	a_1	CH_2CHCH_2 asymmetric CH_2 stretch	3114	25 and 26
2		CH_2CHCH_2 symmetric CH_2 stretch	3052	this work
3		$CH_2(C-H)CH_2$ stretch	3027	this work
4		symmetric CH_2 scissors	1478	this work
5		$CH_2-CH-CH_2$ stretch + CH_2 scissors	1242	this work
6		$CH_2-CH-CH_2$ stretch + CH_2 rock	1068	35
7		$CH_2-CH-CH_2$ bend	425	9 and 10
8	a_2	CH_2CHCH_2 out-of-phase umbrella	775	this work
9		$CH_2-CH-CH_2$ out-of-phase twist	549	35
10	b_1	$CH_2(C-H)CH_2$ out-of-plane bend	983	this work
11		CH_2CHCH_2 in-phase umbrella	802	27
12		$CH_2-CH-CH_2$ in-phase twist	510	this work
13	b_2	CH_2CHCH_2 asymmetric CH_2 stretch	3111	25 and 26
14		CH_2CHCH_2 symmetric CH_2 stretch	3020	this work
15		asymmetric CH/CH_2 scissors	1464	this work
16		asymmetric $CH_2-CH-CH_2$ stretch + CH/CH_2 scissors	1390	this work
17		asymmetric $CH_2-CH-CH_2$ stretch + CH bend	1182	this work
18		asymmetric CH/CH_2 rock		

matrices.[53,54] She concluded that for polyatomic free radicals in Ar matrices the frequency shift is generally less than 1% and usually to the red. Rotationally resolved frequencies are available[25−27] for three of allyl's fundamentals: ν_1 (3113.98488 ± 0.00089 cm^{-1}), ν_{11} (801.71909 ±0.00037 cm^{-1}), and ν_{13} (3110.59857 ± 0.00036 cm^{-1}). The matrix values (from this study) are ν_1 (3109 cm^{-1}), ν_{11} (801 cm^{-1}), and ν_{13} (3107 cm^{-1}). So for the allyl radical, the gas-to-matrix shifts for these three modes are $\Delta\nu_1$ (4 cm^{-1}), $\Delta\nu_{11}$ (0 cm^{-1}), and $\Delta\nu_{13}$ (3 cm^{-1}). Consequently we believe that all of the matrix frequencies for the allyl radical are within ≤1% of the true, gas-phase frequencies.

Finally we recommend a set of vibrational frequencies for the CH_2CHCH_2 radical in Table 5. High-resolution laser absorption spectroscopy[25,26] has established the CH stretching frequencies, ν_1 and ν_{13}, as well as[27] the out-of-plane umbrella mode ν_{11}. Resonance Raman studies[35−37] have observed the a_1 CCC stretching mode ν_6 and the a_2 out-of-phase CH_2 twist ν_9. The low-frequency CCC bending mode ν_7 has been observed[9,10] in the negative ion photodetachment of the allylic anion: $CH_2CHCH_2^- \rightarrow CH_2CHCH_2 + e^-$. All the rest of the frequencies in Table 5 are from this matrix infrared study. Our polarization spectroscopy has provided new information that makes many of CH_2CHCH_2 radical's fundamental assignments more definite. The pulsed nozzle techniques of this paper permit us to produce clean samples of the target allyl radicals. We observe narrow IR absorption lines for CH_2CHCH_2 and these can be measured with high accuracy; consequently, apart from the unknown matrix shifts, the fundamentals are determined to high accuracy.

Acknowledgment. This work was supported by grants from the Chemical Physics Program, United States Department of Energy (DE-FG02-87ER13695 to G.B.E. and DE-FG02-98ER14857 to B.K.C.). G.B.E. also thanks the NSF (CHE-9813659) for support of our surface spectroscopy of organic radicals. The work at NREL was supported by United States Department of Energy Biomass Power program and the National Renewal Energy Laboratory's Directors Discretionary Fund. The Phillip Morris Corporation has suppored part of this work and we thank Dr. Mohammad Hajaligol. Some of the electronic structure calculations were supported by a grant from the National Center for Supercomputer Applications (NCSA Grant CHE-980028n). We are thankful for the excellent workmanship and good humor of Jim Kastengren and Donald David in the CIRES Instrument Design Facility. Finally we acknowledge a pair of reviewers for a careful examination of our manuscript and for several excellent suggestions.

References and Notes

(1) Salem, L. *Pi Electron Theory of Organic Chemistry*; W. A. Benjamin: New York City, 1962.

(2) Salem, L.; Rowland, C. *Angew. Chem., Int. Ed. Engl.* **1972**, *11*, 92.

(3) Ellison, G. B.; Davico, G. E.; Bierbaum, V. M.; DePuy, C. H. *Int. J. Mass Spectrosc. Ion Processes* **1996**, *156*, 109.

(4) The precise formulation of allyl's resonance energy $E_{Res}(CH_2CHCH_2)$ is a subtle issue. This matter is discussed in Section 5 of Ellison, Davico, Bierbaum, and DePuy. One measure of $E_{Res}(CH_2CHCH_2)$ is the rotational barrier of the allylic radical, CH_2CHCHD, which yields a value of 64 ± 4 kJ mol^{-1}. The difference between the bond energies for propane and propene is [(97 ± 2) − (87.4 ± 0.4)] = 10 ± 2 kcal mol^{-1} or 40 ± 9 kJ mol^{-1}.

(5) Houle, F. A.; Beauchamp, J. L. *J. Am. Chem. Soc.* **1978**, *100*, 3290.

(6) Wu, J. C.; Li, R. H.; Chang, J. L.; Chen, Y. T. *J. Chem. Phys.* **2000**, *113*, 7286.

(7) Schultz, T.; Clarke, J. S.; Gilbert, T.; Deyerl, H. J.; Fischer, I. *Faraday Discuss.* **2000**, 17.

(8) Gilbert, T.; Fischer, I.; Chen, P. *J. Chem. Phys.* **2000**, *113*, 561.

(9) Oakes, J. M.; Ellison, G. B. *J. Am. Chem. Soc.* **1984**, *106*, 7734.

(10) Wenthold, P. G.; Polak, M. L.; Lineberger, W. C. *J. Phys. Chem.* **1996**, *100*, 6920.

(11) Baghol-Vayjooee, M. H.; Benson, S. W. *J. Am. Chem. Soc.* **1979**, *101*, 2838.

(12) Friderichsen, A. V.; Radziszewski, J. G.; Nimlos, M. R.; Winter, P. R.; Dayton, D. C.; David, D. E.; Ellison, G. B. *J. Am. Chem. Soc.* **2001**, *123*, 1977.
(13) Friderichsen, A. V. Infrared Spectroscopy of Matrix-Isolated Aromatic Hydrocarbon Radicals. Ph.D. Thesis, Chemistry, University of Colorado, Boulder, CO, 2001.
(14) Kohn, D. W.; Clausberg, H.; Chen, P. *Rev. Sci. Instrum.* **1992**, *63*, 4003.
(15) Chen, P. The Spectroscopy and Photochemistry in Supersonic Jets. Ph.D. Thesis, Chemistry, Yale, 1987.
(16) Brown, A. L.; Dayton, D. C.; Nimlos, M. R.; Daily, J. W. *Chemosphere* **2001**, *42*, 663.
(17) Mamyrin, B. A.; Karataev, V. I.; Shmikk, D. V.; Zagulin, V. A. *Sov. Phys.-JEPT* **1973**, *37*, 45.
(18) Kung, A. H.; Young, J. F.; Harris, S. E. *Appl. Phys. Lett.* 1973.
(19) Berkowitz, J. *Photoabsorption, Photoionization and Photoelectron Spectroscopy*; Academic Press: New York, 1979.
(20) Becke, A. D. *J. Phys. Chem.* **1993**, *98*, 5648.
(21) Becke, A. D. *J. Chem. Phys.* **2000**, *112*, 4020.
(22) Frisch, M. J.; Trucks, G. W.; Schlegel, H. B.; Scuseria, G. E.; Robb, M. A.; Cheeseman, J. R.; Zakrzewski, V. G.; Montgomery, J. J. A.; Stratmann, R. E.; Burant, J. C.; Dapprich, S.; Millam, J. M.; Daniels, A. D.; Kudin, K. N.; Strain, M. C.; Farkas, O.; Tomasi, J.; Barone, V.; Cossi, M.; Cammi, R.; Mennucci, B.; Pomelli, C.; Adamo, C.; Clifford, S.; Ochterski, J.; Petersson, G. A.; Ayala, P. Y.; Cui, Q.; Morokuma, K.; Malick, D. K.; Rabuck, A. D.; Raghavachari, K.; Foresman, J. B.; Cioslowski, J.; Ortiz, J. V.; Baboul, A. G.; Stefanov, B. B.; Liu, G.; Liashenko, A.; Piskorz, P.; Komaromi, I.; Gomperts, R.; Martin, R. L.; Fox, D. J.; Keith, T.; Al-Laham, M. A.; Peng, C. Y.; Nanayakkara, A.; Gonzalez, C.; Challacombe, M.; Gill, P. M. W.; Johnson, B.; Chen, W.; Wong, M. W.; Andres, J. L.; Gonzalez, C.; Head-Gordon, M.; Replogle, E. S.; Pople, J. A. *GAUSSIAN98*, revsion A.7, Gaussian, Inc.: Pittsburgh, PA, 1998.
(23) Pedley, J. B.; Naylor, R. D.; Kirby, S. P. *Thermochemical Data of Organic Compounds*, 3rd ed.; University of Sussex Press: Cambridge, U.K., 1986.
(24) Berkowitz, J.; Ellison, G. B.; Gutman, D. *J. Phys. Chem.* **1994**, *98*, 2744.
(25) Uy, D.; Davis, S.; Nesbitt, D. J. *J. Chem. Phys.* **1998**, *109*, 7793.
(26) DeSain, J. D.; Thompson, R. I.; Sharma, S. D.; Curl, R. F. *J. Chem. Phys.* **1998**, *109*, 7803.
(27) Hirota, E.; Yamada, C.; Okunishi, M. *J. Chem. Phys.* **1992**, *97*, 2963.
(28) Hirota, E. *J. Mol. Struct.* **1994**, *320*, 75.
(29) Heller, C.; Cole, T. *J. Chem. Phys.* **1962**, *37*, 243.
(30) Krusic, P. J.; Kochi, J. K. *J. Am. Chem. Soc.* **1968**, *90*, 7.
(31) Hudgens, J. W.; Dulcey, C. S. *J. Phys. Chem.* **1985**, *89*, 1505.
(32) Minsek, D. W.; Blush, J. A.; Chen, P. *J. Phys. Chem.* **1992**, *96*, 2025.
(33) Minsek, D. W.; Chen, P. *J. Phys. Chem.* **1993**, *97*, 7.
(34) Sappey, A. D.; Weisshaar, J. C.*J. Phys. Chem.* **1987**, *91*, 3731.
(35) Getty, J. D.; Burnmeister, M. J.; Westre, S. G.; Kelly, P. B. *J. Am. Chem. Soc.* **1991**, *113*, 801.
(36) Getty, J. D.; Kelly, P. B. *Chem. Phys.* **1992**, *168*, 357.
(37) Getty, J. D.; Liu, X.; Kelly, P. B. *Chem. Phys. Lett.* **1993**, *201*, 236.
(38) Liu, X.; Getty, J. D.; Kelly, P. B. *J. Chem. Phys.* **1993**, *99*, 1522.
(39) Holtzhauer, K.; Cometta-Morini, C.; Oth, J. F. M. *J. Phys. Org. Chem.* **1990**, *3*, 219.
(40) Huang, J. W.; Graham, W. R. M. *J. Chem. Phys.* **1990**, *93*, 1583.
(41) Maier, G.; Reisenauer, H. P.; Rohde, B.; Dehnicke, K. *Chem. Ber.* **1983**, *116*, 732.
(42) Mal'tsev, A. K.; Korolov, V. A.; Nefedov, O. M. *Bull. Acad. Sci. USSR, Chem. Ser.* **1983**, *31*, 2131.
(43) Mal'tsev, A. K.; Korolov, V. A.; Nefedov, O. M. *Bull. Acad. Sci. USSR, Chem. Ser.* **1984**, *33*, 510.
(44) Currie, C. L.; Ramsay, D. A. *J. Chem. Phys.* **1966**, *45*, 488.
(45) Callear, A. B.; Lee, H. K. *Trans. Faraday Soc.* **1968**, *64*, 308.
(46) Ha, T. K.; Baumann, H.; Oth, J. F. M. *J. Chem. Phys.* **1986**, *85*, 1438.
(47) Blush, J. A.; Minsek, D. A.; Chen, P. *J. Phys. Chem.* **1992**, *96*, 10150.
(48) Michl, J.; Thulstrup, E. W. *Spectroscopy with Polarized Light*; VCH Publishers, Inc.: New York, 1996.
(49) Ball, D. W.; Pong, R. G. S.; Kafafi, Z. H. *J. Am. Chem. Soc.* **1993**, *115*, 2864.
(50) Cyvin, S. J. *J. Chem. Phys.* **1958**, *29*, 583.
(51) Woodfin, E. S.; Fletcher, W. H. *J. Mol. Spectrosc.* **1957**, *1*, 95.
(52) Davis, S. High-Resolution Infrared Spectroscopy of Slit-Jet Cooled Transient Molecules: From van der Waals clusters, to Hydrogen Bound Dimers to Small Organic Radicals. Ph.D. Thesis, Chemistry, University of Colorado, Boulder, CO, 1999.
(53) Jacox, M. E. *J. Mol. Spectrosc.* **1985**, *113*, 286.
(54) Jacox, M. E. *Chem. Phys.* **1994**, *189*, 149.
(55) Jacox, M. E. *Vibrational and Electronic Energy Levels of Polyatomic Transient Molecules*; American Chemical Society: Gaithersburg, Maryland, 1994.